



Air-cladded mode-group selective photonic lanterns for mode-division multiplexing

Mariam Mathew, Neethu; Christensen, Jesper Bjerger; Grüner-Nielsen, Lars; Galili, Michael; Rottwitt, Karsten

Published in:
Optics Express

Link to article, DOI:
[10.1364/OE.27.013329](https://doi.org/10.1364/OE.27.013329)

Publication date:
2019

Document Version
Publisher's PDF, also known as Version of record

[Link back to DTU Orbit](#)

Citation (APA):
Mariam Mathew, N., Christensen, J. B., Grüner-Nielsen, L., Galili, M., & Rottwitt, K. (2019). Air-cladded mode-group selective photonic lanterns for mode-division multiplexing. Optics Express, 27(9), 13329-13343 .
<https://doi.org/10.1364/OE.27.013329>

General rights

Copyright and moral rights for the publications made accessible in the public portal are retained by the authors and/or other copyright owners and it is a condition of accessing publications that users recognise and abide by the legal requirements associated with these rights.

- Users may download and print one copy of any publication from the public portal for the purpose of private study or research.
- You may not further distribute the material or use it for any profit-making activity or commercial gain
- You may freely distribute the URL identifying the publication in the public portal

If you believe that this document breaches copyright please contact us providing details, and we will remove access to the work immediately and investigate your claim.

Air-cladded mode-group selective photonic lanterns for mode-division multiplexing

NEETHU MARIAM MATHEW,^{1,*} JESPER BJERGE CHRISTENSEN,¹
LARS GRÜNER-NIELSEN,^{1,2} MICHAEL GALILI,¹ AND KARSTEN
ROTTWITT¹

¹DTU Fotonik, Ørstedss Plads, Building 343, 2800 Kgs. Lyngby, Denmark

²Danish Optical Fiber Innovation, Åveningen 22A, 2700 Brønshøj, Denmark

*namama@fotonik.dtu.dk

Abstract: We have fabricated an air-cladded mode-group selective photonic lantern, which can (de)multiplex the first two mode groups of a standard two-mode step-index fiber. Instead of relying on a low-index capillary tube, our simple solution uses air to form the surrounding “cladding” and thereby enables guiding at the end of the taper. Characterization of a 25-mm long lantern taper results in multiplexing crosstalk values between -20 dB and -12 dB for both modal inputs. The de-multiplexing values were around -12 dB for the fundamental mode, and slightly higher for the first higher-order (LP₁₁) mode. Microscopic imaging of a taper cross section having a width of 30 μm reveals the presence of an uncollapsed airhole in the structure between the three fibers. The impact of such an airhole is numerically investigated using an eigenmode expansion method based on a full-vectorial mode solver, and is found to play an important role in assuring a more adiabatic mode conversion through the taper.

© 2019 Optical Society of America under the terms of the [OSA Open Access Publishing Agreement](#)

1. Introduction

Optical communication using single mode fibers is approaching the fundamental limits imposed by signal to noise ratio and non-linearity [1]. Space division multiplexing (SDM) exploits the last available dimension using multi-core fibers or multimode fibers [2]. Few mode fibers, which can support the first few modes, typically 2-12 modes, can be used in mode division multiplexing (MDM), where independent signals are transmitted simultaneously in separate spatial modes [3]. Incorporating MDM technology together with the existing wavelength or polarization multiplexed signals further multiplex the number of transmitted channels with the number of spatial modes used in transmission. One of the main challenges of MDM is the efficient combining and splitting of different spatial modes with low crosstalk. Multiple-input multiple-output (MIMO) processing circuits can be used to compensate crosstalk [3], but the implementation is expensive and complicated. Excitation of higher order modes in a few mode fiber can, for example, be achieved using spatial light modulators (SLM) [4], but SLMs require free space coupling, which is cumbersome. Fiber based long period gratings (LPG) can also excite higher order modes but they have bandwidth limitations. Furthermore, SLM and LPG are single channel devices, and so to excite different higher order modes simultaneously, one has to cascade more of these devices, resulting in increased loss. Thus we are in need of low loss, wide bandwidth, fiber based mode multiplexers. Photonic lanterns have emerged as a suitable alternative here [5].

Photonic lanterns can transform light from different single mode waveguides to a multi-mode waveguide and vice versa. The transformation happens through a tapered mode transition, which should be sufficiently long to enable adiabatic conversion [6]. Usually photonic lanterns are fabricated by inserting the single mode fibers (SMFs) in a low refractive index fluorine-doped capillary tube, and the whole structure is then tapered down [7]. A multi-mode waveguide is formed at the tapered end with the single mode fiber claddings forming the new core and the low index capillary tube forming the new cladding. In a standard photonic lantern the single

mode fibers used are identical and there would not be one to one correspondence between the single mode cores and the modes at the multi-mode end. When light is coupled to any of the SMFs, one gets a linear combination of the available multi-mode waveguide modes at the tapered end. If photonic lanterns have to be used without MIMO components, then it is required to excite a specific mode by coupling light through a specific single mode fiber. Such mode selectivity can be attained by introducing dissimilarity between the single mode fibers either in core size or refractive indices. Degenerate LP modes with the same propagation constants need not be excited separately as they will couple to each other in the few mode fiber. Such mode-group selective lanterns that could excite up to the first four LP mode groups have been recently demonstrated [8,9].

The capillary tubes used in the lantern fabrication need to have a lower refractive index than the silica cladding to ensure wave guiding at the tapered multi-mode end. These capillary tubes are not that easily accessible. Moreover, as the number of single mode fibers increase, a larger capillary tube is needed and uniform tapering in the glass processor becomes difficult and expensive especially if a heating filament unit is used for tapering. Hence, we have suggested a fabrication technique that circumvents the use of a capillary tube [10]. In this paper, we describe our new technique and characterize the fabricated lanterns. The experimental results are backed up by modelling, using a 2-D scalar mode solver in section 2 and a 3-D full-vectorial eigenmode expansion method in section 4.

2. New fabrication technique

A Vytran filament glass processor is used for the fabrication of lanterns. Three single mode fibers are crossed together and held under tension between the fiber holding blocks of the splicer and axially heated, so the fibers melt together. The melted fiber bundle is then tapered down and cleaved at the taper waist. The cleaved fiber bundle is spliced to a few mode fiber. The air surrounding the taper form the new cladding at the multi-mode end of the taper. A schematic of the proposed lantern is shown in Fig. 1. To make the air-cladded photonic lantern mode selective

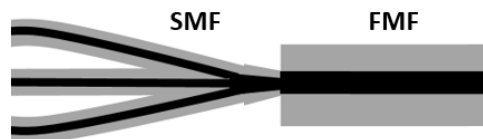


Fig. 1. A schematic of the new fabrication technique.

between the first two LP mode groups, two different types of fibers are used [11]. One is a standard single mode fiber (SSMF) with core diameter of 9 μm and core index 1.4492, while the other two are low cut-off fibers (Corning HI1060) of core diameter 5.3 μm and core index 1.4511. The cladding index is 1.4444 for both fibers (all index values measured at 1550 nm). The light coupled into the big core evolves to the LP_{01} -like mode and light coupled into either of the HI1060 fibers should evolve into a linear combination of LP_{11a} and LP_{11b} -like modes.

A 2-D scalar mode solver is programmed and used to model the lantern at a wavelength of 1550 nm. The three fiber cores are arranged at the vertices of an equilateral triangle and an air cladding surrounds the three fibers. The modelled effective index values of the first 6 lantern modes along the taper is shown in Fig. 2. Lantern mode 1 starts in the SSMF, while mode 2 and 3 are the even and odd supermodes of the HI1060 fibers. Mode 4 and beyond are the unused guided cladding modes. The mode profiles of the first six lantern modes obtained at the end of the taper is also shown in Fig. 2. A slow and gradual taper ensures that, the power coupled into SSMF stays in mode 1, while power coupled to the two HI1060 fibers stays within modes 2 and 3.

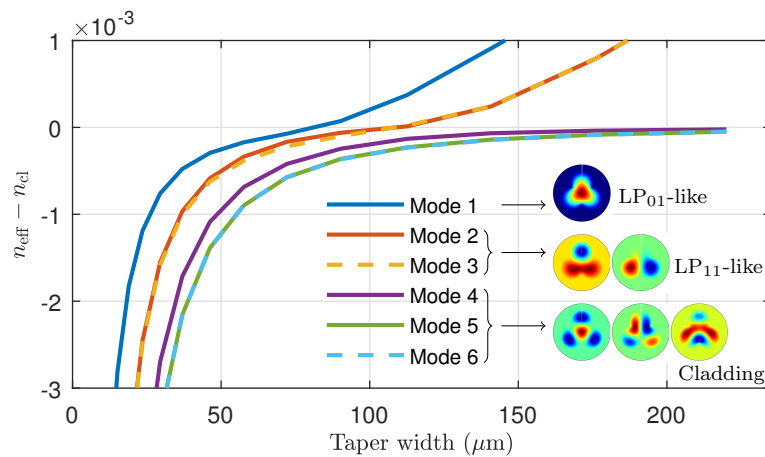


Fig. 2. Modelling of effective index variation of the lantern modes along the taper at 1550 nm. The mode distribution at a taper width of 23 μm is inserted.

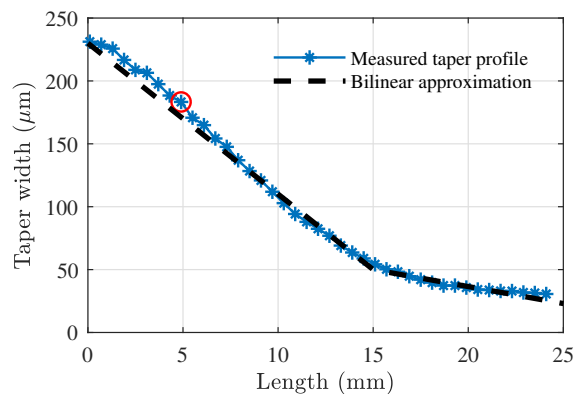


Fig. 3. A typical taper profile of a 25 mm long taper. The bi-linear approximation used for 3D simulations is superimposed.

A taper length of 20 mm is fabricated [12], and the taper is cleaved at the middle of the 10 mm long waist part of the taper, yielding a total lantern taper length of 25 mm. As there is no capillary tube to hold the fibers together, the SMFs are crossed together and heated axially before tapering [13]. Though the fibers are crossed before heating, after the taper, the SMFs stay straight in most of the taper region as shown in Fig. 4(a), which is a short taper of length 1 mm. This is further confirmed by inspecting the entire 20 mm taper region, and the width of the taper along the taper length is also measured as shown in Fig. 3. The red circle shows the point below which the fibers stay crossed. This point is far prior to the coupling region of the taper, and the light is well confined within the SMF cores. The profile shows that the taper is not linear. The taper is more gradual and slow where the taper width varies from 50 μm to 25 μm . Consequently we use a bi-linear approximation for the 3-D simulation in section 4 as shown in Fig. 3.

The cleaved tapered end is spliced to an OFS two mode step index fiber (TMF) of core diameter 19 μm , which can support the first two LP mode groups. This is a dissimilar splice between the 125 μm TMF and the taper end of around 20 μm . An image of such a splice is shown in Fig. 4(b). The end view images give the cross section at the tapered end as shown in Fig. 5, and

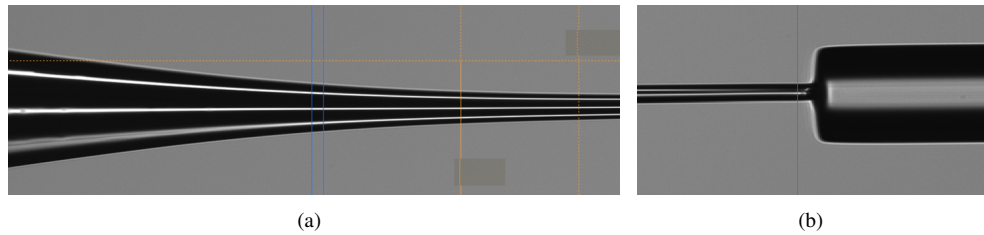


Fig. 4. (a) Three fiber bundle taper. (b) Dissimilar splice between the fiber bundle and few mode fiber.

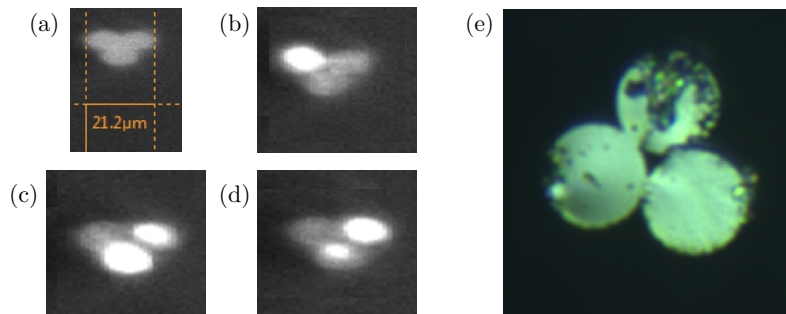


Fig. 5. Cross section image of the tapered end of three fiber bundle taken using (a) the Vytran camera with background light, (b) white light coupled into the SSMF, (c) one of the HI1060 fibers (d) the other HI1060 fiber, and (e) a microscope image of a taper cross section of width 33 μm.

the final taper width is measured to around 21 μm. The three fibers are well fused together. The cross section images are also taken, with white light coupled into each of the input SMFs. White light coupled into the big core SSMF preferentially stays in the same core, while light coupled into either of the small core HI1060 fibers, couple with the other HI1060 fiber as shown in Fig. 5. Compared to the simulated eigenmodes at 1550 nm shown in Fig. 2, the field from white light is, as expected, more confined within the individual fibers because of the lower wavelength of white light. A microscope image of a taper end of width 33 μm is shown in Fig. 5. At this width, an air hole is visible in the structure.

The power coupling between the tapered fiber bundle end and the TMF plays a major role in the performance of the lantern. This power coupling can be calculated using the overlap integral between the first three lantern modes and the corresponding TMF modes. The modes are calculated using the 2D scalar mode solver. The overlap loss is found to be minimum around a taper width of 23 μm as shown in Fig. 6(a), and hence the three-fiber bundle is tapered down to approximately this size. Moreover, the dissimilar splice alignment is very critical. The effect of splice misalignment on the crosstalk is simulated using the scalar model and shown in Fig. 6(b). Here crosstalk is defined as the ratio of the power in unwanted modes to the total power in all modes. The splice offset is modelled by displacing the TMF from the center, at an angle of 45°. The variation of crosstalk of the LP_{01} and LP_{11} modes with splice offset depends on the direction of offset. At 90° angle, the crosstalk on LP_{11x} is very small, while LP_{01} and LP_{11y} are higher. At 180° angle, the crosstalk on LP_{11y} is small, while LP_{01} and LP_{11x} are higher. However, at all angles the crosstalk on LP_{01} remains slightly higher than the LP_{11} modes and this is due to the non circular shape of the tapered end.

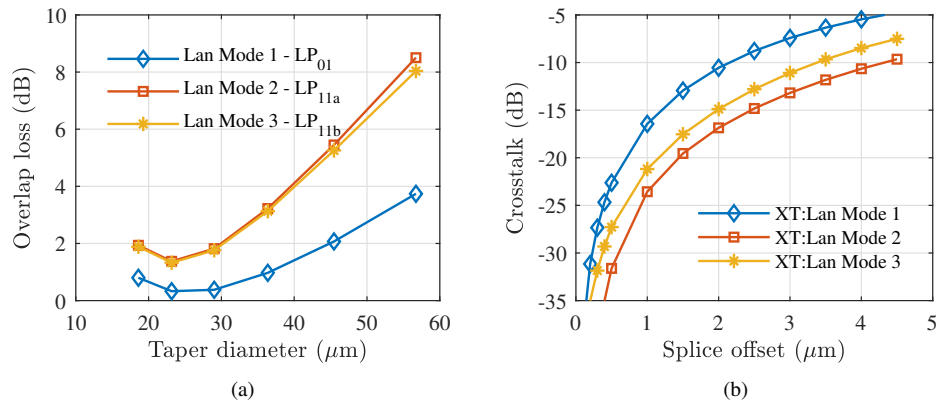


Fig. 6. (a) Modelled overlap loss as a function of taper diameter. (b) Modelled effect of crosstalk on splice offset.

The finished lantern is fixed on a plastic base as shown in Fig. 7 so that it remains stable while being characterized. For the future, it is the plan to develop a smaller, more stable and protective packaging.

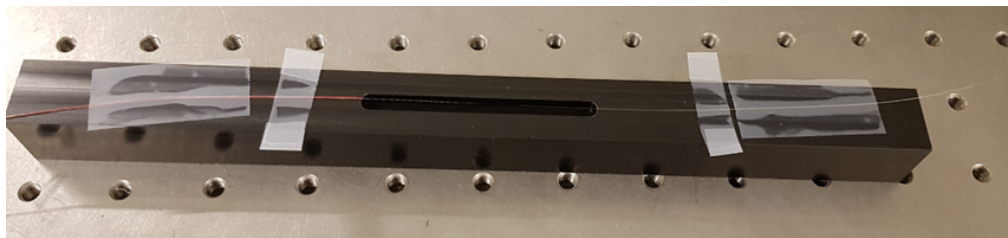


Fig. 7. The final fabricated photonic lantern on a plastic base.

3. Characterization of the fabricated photonic lantern

The fabricated lanterns are first characterized by loss measurements. This characterization is performed both in the multiplexing direction, i.e. from the SMFs to the TMF, and in the de-multiplexing direction, i.e. from the TMF to the SMFs.

To obtain the multiplexing loss, the light from a tunable laser is coupled into each of the three SMFs of the lantern, and the output power of the TMF is measured. To obtain the polarization dependence of the loss, the polarization scanning method [14] is used where light from the tunable laser is sent through an electrically controlled polarization controller, which scans the whole Poincaré sphere in less than 10 seconds, before it is fed into the SMFs. The wavelength of the tunable laser is varied from 1524 nm to 1576 nm, while scanning the polarization at each wavelength. The minimum (blue line) and maximum loss (red line) measured at each wavelength for the three different SMF inputs is shown in Fig. 8. The multiplexing loss for the HI1060 fiber input is larger than the SSMF input. This difference in loss is due to different mode overlaps at the splice between the taper end and the TMF. This is confirmed by butt coupling the taper end and the TMF at different alignment positions while measuring the multiplexing loss in each case as given at the end of this section. A lower SSMF input loss often shows a higher crosstalk on

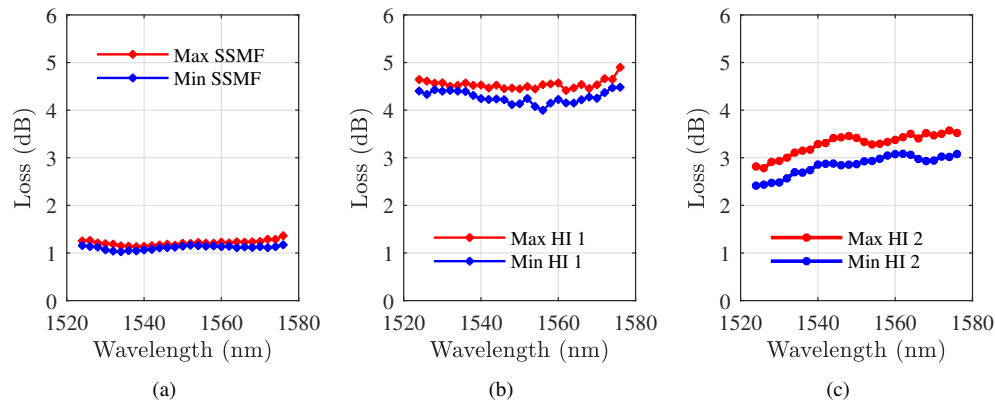


Fig. 8. Polarization dependent multiplexing loss when light is coupled to (a) the SSMF (b) one HI1060 (c) the other HI1060. Loss is calculated from the power measured at the two mode fiber.

the LP_{01} mode.

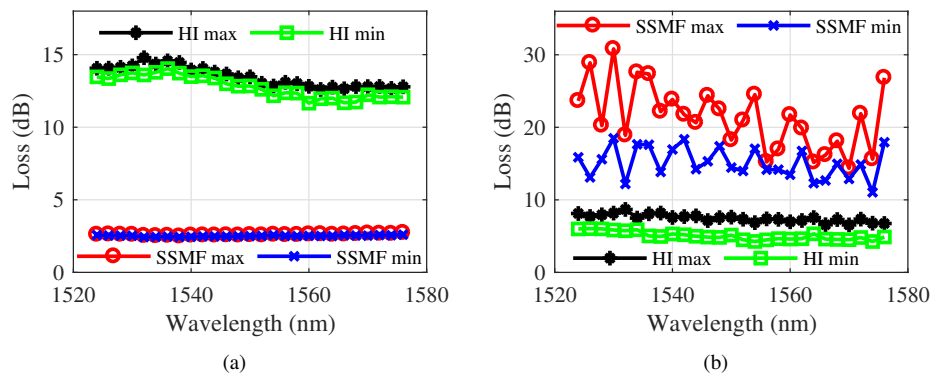


Fig. 9. Polarization dependent de-multiplexing loss when (a) LP_{01} mode (b) LP_{11} mode is launched into the two mode fiber. Loss is calculated from the power measured at the SSMF and the sum of powers at the two HI1060 fibers.

To measure the de-multiplexing loss, first an LP_{01} mode is launched into the TMF through a splice to an SMF pigtailed fiber. To further suppress higher-order modes in the TMF, a mode stripper is used, resulting in the LP_{11} mode being suppressed by at least 40 dB in total. The output power is measured at the three SMFs. Ideally the power at the SSMF end gives the amount of light in the LP_{01} mode, and the power in the LP_{11} mode will be distributed into a linear combination of light in the two HI1060 fibers. Hence, the power in the SSMF, and the sum of powers in the HI fibers, are used to quantify the de-multiplexing performance of the lantern as shown in Fig. 9(a). The difference between the two losses gives a measure of the LP_{01} de-multiplexing crosstalk, which is measured to -11.5 dB at 1550 nm. The polarization dependence of the LP_{11} power is shown by the green and black lines in Fig. 9(a), and is 1.2 dB at 1550 nm.

Next, the LP_{11} mode is launched into the TMF, using a thermally induced LPG, where the

LP_{01} is suppressed more than 15 dB in the wavelength range used here [15]. The polarization dependent output power at the SSMF and the linear sum of power at the two HI1060 fibers are measured as before and shown in Fig. 9(b). At the worst polarization the LP_{11} cross talk is -6.8 dB, while for the best polarization it goes as low as -13 dB. The polarization dependence of loss is larger for the LP_{11} launch. Depending on the input polarization, the orientation of LP_{11} mode in the TMF changes and hence the overlap with the modes at the tapered end also changes and this affects the loss. Repeating the measurement on a finer wavelength range reveals that the large variation in the SMF loss in Fig. 9(b) is due to the modal interference between the LP_{01} and LP_{11} mode [16]. The LPG has a higher suppression ratio of 25 dB around 1550 nm and hence the amplitude of oscillation is lower at the center. Both the multiplexing and de-multiplexing loss is seen to be largely wavelength independent over the C-band.

A spatial and spectral (S^2) [17] imaging set up is used to get the mode images at the TMF end and to measure the multiplexing crosstalk. As shown in Fig. 10, the light from the tunable source is fed to each of the SMFs through a polarization controller. The near field distribution at the TMF end of the lantern is captured using an infrared camera, while scanning the wavelength over a 10 nm range. From the wavelength dependence of these captured fields, the generated dominant mode and the crosstalk from the other mode is calculated [17]. When light is coupled to the large core SSMF, the dominant mode at the TMF end is LP_{01} and when light is coupled to either of the small core HI1060 fibers, the dominant mode is a linear combination of the LP_{11a} and LP_{11b} modes. The input polarization of each SMF is randomly varied ten times and the dominant mode profile at the TMF is found and the crosstalk from the other mode is calculated. The results for five out of ten different polarizations are shown in Table 1. For each SMF input, the dominant mode at the two mode fiber and the calculated crosstalk from the other mode is shown. The crosstalk varies with input polarization. Here the wavelength range used is 1545 nm to 1555 nm with a wavelength step of 0.2 nm. The wavelength range and step size used for S^2 imaging is optimized for a TMF length of 3.5 m.

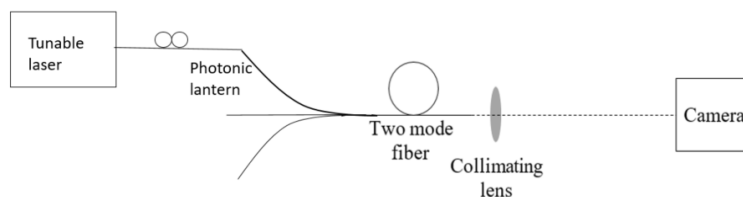
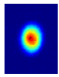
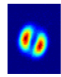
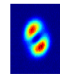
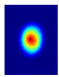
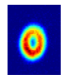
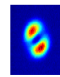
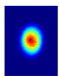
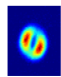
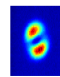
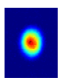
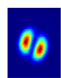
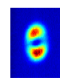
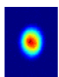
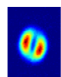
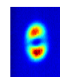


Fig. 10. S^2 imaging set up used for the characterization of the lantern.

The wavelength used for S^2 imaging is also changed and the above measurements are repeated and the results are shown in Fig. 11. The measured crosstalk for the three SMF inputs at 10 different polarizations are plotted at the average wavelength used for S^2 imaging. The results show that the crosstalk is largely wavelength independent over the C-band. Table 1 and Fig. 11 show that the crosstalk is different when light is coupled to each of the three SMF fibers. This is the first time that a fabricated photonic lantern is characterized by S^2 imaging technique.

To understand more about this crosstalk variation, a new set of measurements are done using a 25 mm long three fiber taper, butt-coupled to a TMF. S^2 measurements for 10 different polarizations are repeated at two different alignment positions for the butt-coupling. The polarization dependent multiplexing loss is also measured at these positions and the results are shown in Table 2. The alignment position is determined by measuring the offset from the center of the TMF using the camera of the glass processor. For the first alignment position, the offset is measured as 1.9 μm . When light is coupled to the SSMF, the multiplexing loss varies from 3 dB to 3.4 dB and S^2 measurements show that one of the HI1060 input coupling gives the

Table 1. S^2 imaging in the Multiplexing direction at different Polarizations.

SSMF Input		First HI1060 Input		Second HI1060 Input	
Dominant mode	Crosstalk	Dominant mode	Crosstalk	Dominant mode	Crosstalk
	-13.9 dB		-11.7 dB		-17.8 dB
	-14.6 dB		-12.1 dB		-18.5 dB
	-14.7 dB		-12.5 dB		-19.9 dB
	-15.7 dB		-13.3 dB		-20.5 dB
	-17.8 dB		-13.7 dB		-21.7 dB

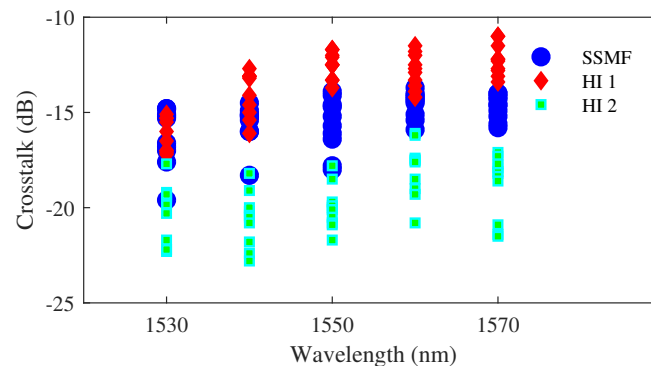


Fig. 11. The measured crosstalk of the fabricated lantern at different wavelengths.

highest crosstalk of -10.7 dB. For the second alignment, the tapered end is slightly moved from the center of the TMF, and the offset measured is 2.9 μm . The multiplexing loss for the SSMF input decreases to 1.4 dB to 1.7 dB, while the crosstalk on SSMF input increases to -8.2 dB. This shows that the crosstalk of the lantern depends much on the alignment between the tapered end and the TMF. The effect is more pronounced for the SSMF input than the HI fiber input, in agreement with the modelled result shown in Fig. 6(b). Hence, it is beneficial to optimize the alignment position to minimize the crosstalk for all three input SMFs, before performing the dissimilar splice.

To demonstrate the capability of the lantern to do mode division multiplexing, two of these air clad lanterns are used as multiplexer and de-multiplexer in a transmission experiment set up as shown in Fig. 12. Two SDM channels are transmitted simultaneously up to 20 km [18]. The

Table 2. Measured Polarization dependent Multiplexing Loss and Crosstalk on a butt-coupled lantern.

Input fibers	Alignment 1 offset: 1.9 μm		Alignment 2 offset: 2.9 μm	
	Mux loss dB	Crosstalk dB	Mux loss dB	Crosstalk dB
SSMF	3 to 3.4	-17.3 to -12.2	1.4 to 1.7	-13.4 to -8.2
HI1	5.2 to 6.1	-22.9 to -17.2	4 to 5.8	-15.4 to -12.7
HI2	4.8 to 5.7	-13.8 to -10.7	5.2 to 6.4	-14.4 to -11.8

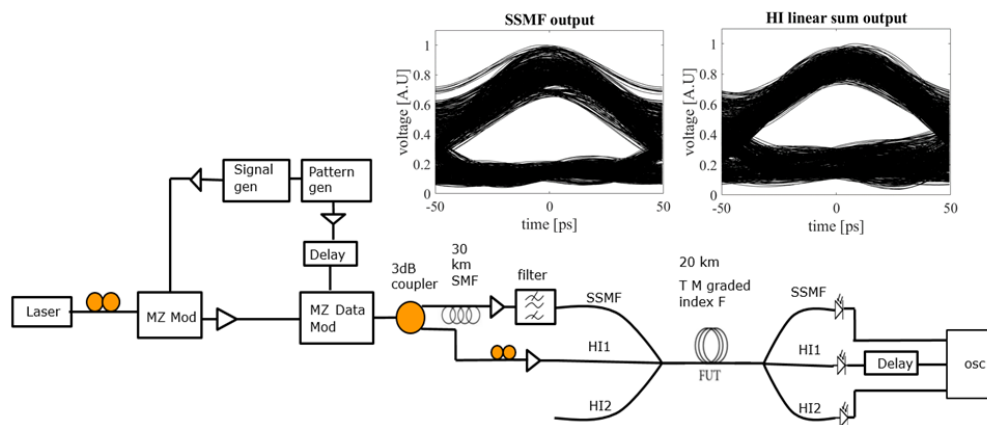


Fig. 12. Experimental setup used for the data transmission.

polarization-dependent loss and crosstalk of the individual lanterns impacts the transmission performance as well. For the best input polarization, a high Q value between 4.5 and 6.5 is observed, while at certain other polarizations the signal degrades to a Q of 2.6. The eye diagrams obtained for the best input polarization for the LP_{01} and LP_{11} channel are shown in Fig. 12. The results show that the fabricated lanterns could be used for SDM transmission without MIMO processing, but the polarization dependence of crosstalk and loss of the lanterns, need to be reduced.

4. Simulations: the eigenmode expansion method

This far the lantern taper was analysed using a 2-D scalar mode solver to obtain the effective refractive indices of the local eigenmodes at different cross sections throughout the taper. To further improve our understanding of the taper part of the structure, we now numerically analyse the lantern taper based on the eigenmode expansion (EME) method; a rigorous approach for solving Maxwell's equations. The simulations are carried out using a commercial full-vectorial

finite-difference eigenmode (FDE) solver and EME propagator [19]. To the best of our knowledge, this is the first time this method has been used to simulate light propagation in photonic lantern structures.

The full vectorial EME method relies on a decomposition of the electromagnetic field in a basis of eigenmodes (guided and non-guided), computed on a 2-D cross-sectional grid. In non-uniform structures, as found in tapers, the (local) eigenmodes change along the direction of propagation, z . The EME method deals with this by partitioning the taper structure into M longitudinally uniform subsections (of potentially varying lengths z_m), in each of which N local eigenmodes are computed. Neighbouring sections are ‘stitched’ together through the interface scattering matrices $S_{m,m+1}$, which are computed based on the electromagnetic boundary conditions and modal-overlap calculations [20].

Among the outputs of the EME simulation is the system scattering matrix S . The components of S are complex valued coefficients s_{jk} , which quantify the conversion from eigenmode j at the taper input to eigenmode k at the taper output. Thus, from S one may easily extract important quantities such as the mode-dependent loss and mode-dependent crosstalk. Moreover, the EME method provides the scattering coefficients from an arbitrary eigenmode at the input to the N eigenmodes in every subsection along the taper. This functionality facilitates analysis of light propagation through the lantern taper, and is, in particular, useful if the mode conversion is non-adiabatic as it helps identifying the region(s) along the taper where the crosstalk occurs.

To limit computation time and memory costs, we utilize that the considered lantern taper features a symmetry plane mirroring the two HI1060 fibers. By making use of this symmetry, we not only halve the size of the 2-D computational grid, but also halve the number of eigenmodes, i.e. $N \rightarrow N/2$. This simplification is justified by the fact that even and odd eigenmodes with respect to the symmetry axis will not couple to each other, thus allowing us to include only the even (or the odd) eigenmodes. In all simulations below, we use the same core sizes and core and cladding indices as for the 2-D scalar simulation in section 2. Furthermore, we use a bi-linear taper profile (shown in Fig. 3) consisting of a 15 mm taper from the initial width $d_1 = 225 \mu\text{m}$ to $50 \mu\text{m}$ followed by a 10 mm taper down to the final taper width $d_2 = 23 \mu\text{m}$. The simulated structures are shown in the insets of Figs. 15(a) and 16(a).

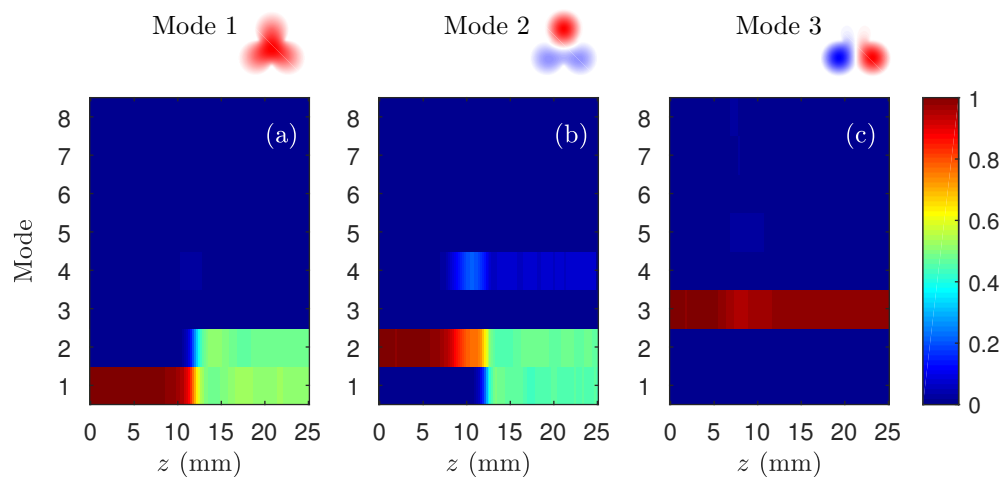


Fig. 13. Relative power distribution versus taper distance in a 25-mm air-cladded 3-core lantern bi-linear taper. The initial light distribution is given by (a) eigenmode 1, (b) eigenmode 2, and (c) eigenmode 3, shown at the taper endpoint above each subfigure.

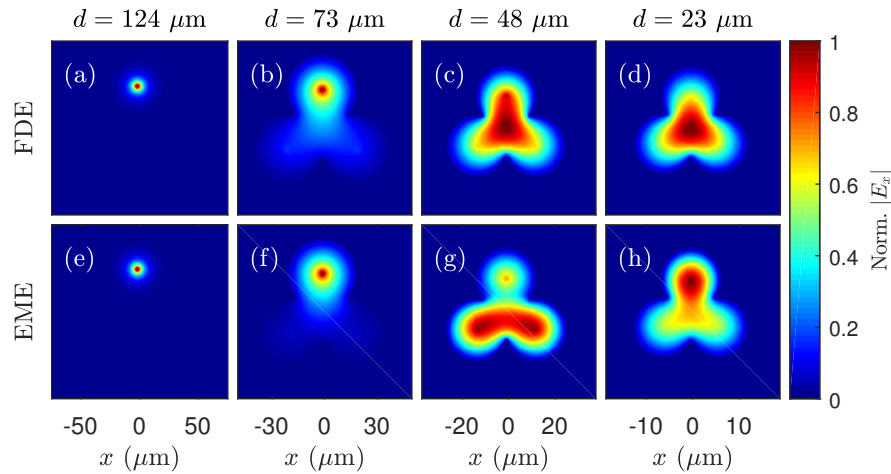


Fig. 14. Fundamental eigenmode (a-d) and EME-propagated field (e-h) at four different locations along the 25-mm long lantern bi-linear taper. The deviation between the EME propagated field and the local eigenmodes indicates non-adiabatic mode conversion. The y-axis (not shown) is for each subfigure identically scaled as the corresponding x-axis.

4.1. Conventional lantern taper

Figure 13 shows the EME-calculated modal power distribution as a function of taper distance starting at the taper input with the three lowest lantern eigenmodes. First, Fig. 13(c) illustrates that the odd LP_{11} -like supermode (mode 3) is almost perfectly adiabatically converted along the taper. It only exhibits weak coupling to higher-order modes, and no coupling at all to modes 1 and 2 as a result of the symmetry in the structure [see Eq. (1) below]. On the other hand, the simulation predicts strong mode coupling (i.e. strongly non-adiabatic mode conversion) between the LP_{01} -like mode (mode 1) and the even LP_{11} -like supermode (mode 2). The mode crosstalk occurs in a specific part of the taper after a length of 9 – 13 mm, corresponding to a taper diameter in the range of 50 – 90 μm . In the remaining (10 mm) part of the bi-linear taper, the mode conversion appears to be adiabatic, owing to the decreased taper angle. Notably, mode 2 experiences a larger loss due to higher-order-mode coupling, which is in agreement with the mode-dependent loss experimentally observed (see section 3).

To exemplify the non-adiabatic mode conversion, Fig. 14 illustrates how light launched in the unique SSMF core evolves as it propagates through the lantern taper. The EME-propagated electric field [Fig. 14(e-h)] is shown at four different locations along the taper together with the corresponding fundamental eigenmode [Fig. 14(a-d)]. Ideally, the EME-propagated field would at all positions resemble the local eigenmode. The large deviation between subfigures (c) and (g), therefore, indicates non-adiabatic mode conversion as the structure is tapered from $d = 73 \mu\text{m}$ to $d = 48 \mu\text{m}$.

Local adiabatic conversion requires (local) fulfillment of the weak power transfer criterion [6, 21, 22]

$$\eta(z) = \frac{2\pi}{\Delta\beta} \frac{d\rho}{dz} \left| \int_A \psi_1(x, y, z) \frac{\partial \psi_2(x, y, z)}{\partial \rho} dA \right| \equiv \frac{2\pi}{\Delta\beta} \frac{d\rho}{dz} \kappa(z) \ll 1, \quad (1)$$

in which $\Delta\beta \equiv \beta_1 - \beta_2$ is the difference in propagation constant of the relevant local eigenmodes $\psi_{1,2}$ (normalized such that $\int_A |\psi_{1,2}|^2 dA = 1$), κ is defined as the modal overlap between ψ_1 and $\partial\psi_2/\partial\rho$, and, finally, $\rho(z)$ is a parameter which quantifies the cross-sectional size of the lantern

taper, taken to be its width d . Equation (1) expresses that the degree of local mode coupling depends on two factors: Firstly, the difference in the propagation constants of the two modes, and secondly, the size of the overlap between one of the eigenmodes and the longitudinal change of the other eigenmode [23]. The latter is directly related to the (local) taper angle ($d\rho/dz$), and generally becomes considerable in the part of the taper where the eigenmodes expand beyond their original cores.

To further investigate the simulated lantern taper, Fig. 15 illustrates the effective refractive index of the three lowest order eigenmodes along the taper, the overlap integral κ , and the parameter η . The effective index curves are almost identical to those obtained by the scalar mode solver (see Fig. 2) confirming its approximate validity. Notably, the part of the taper that exhibits a significant coupling coefficient κ coincides with the part of the taper where the modal effective indices approach each other ($d \approx 70 \mu\text{m}$). The result of this is that η grows beyond unity for both a linear taper (i.e. constant taper angle of $\theta \approx d\rho/dz = 0.08 \text{ rad}$) and the bi-linear taper from Fig. 3 (with $\theta_1 \approx 0.12 \text{ rad}$ down to a taper width of $50 \mu\text{m}$ and $\theta_2 \approx 0.02 \text{ rad}$ down to the final taper width of $23 \mu\text{m}$). While this is in agreement with the non-adiabatic mode conversion seen in Figs. 13 and 14, the strongly non-adiabatic conversion in the taper is surprising, given the low crosstalk values obtained experimentally.

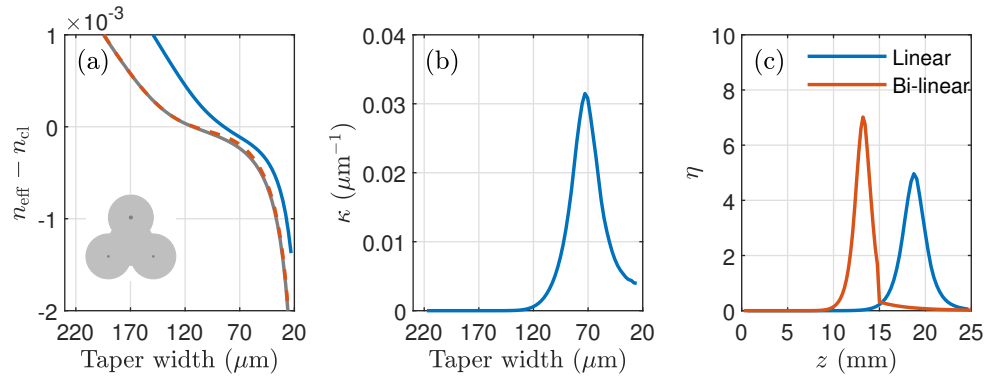


Fig. 15. (a) Effective index curves versus taper width for the three lowest eigenmodes. (b) Local coupling coefficient κ , and (c) the parameter η for both a linear 25 mm taper and the considered bi-linear 25 mm taper.

4.2. Air-holed lantern taper

For a taper cross section of width $30 \mu\text{m}$ and above, an uncollapsed airhole is observed as shown in Fig. 5. We included such an air hole in our simulations and computed both the effective refractive index [see Fig. 16(a)] and coupling integral κ [see Fig. 16(b)] versus taper diameter. In comparison with the conventional lantern taper, the air-hole lantern taper exhibits a smaller differential effective index towards the end of the taper. At first sight this might suggest that the air-holed structure is more prone to mode coupling. However, as seen in Fig. 16(b), the coefficient κ peaks at a lower taper width, and with a lower value, than obtained for the conventional lantern taper [see Fig. 15(b) for comparison]. This behavior is explained by the air hole acting to suppress (delay) modal expansion, or, in other words, the three fibers to a larger extent behave like three individual waveguides. As seen in Fig. 16(c) the resulting local conversion parameter η is smaller than that obtained for the conventional lantern taper. This is especially the case for the bi-linear taper for which the coupling integral is predominantly large only in the second part of the taper ($z > 15 \text{ mm}$) where the tapering angle is low.

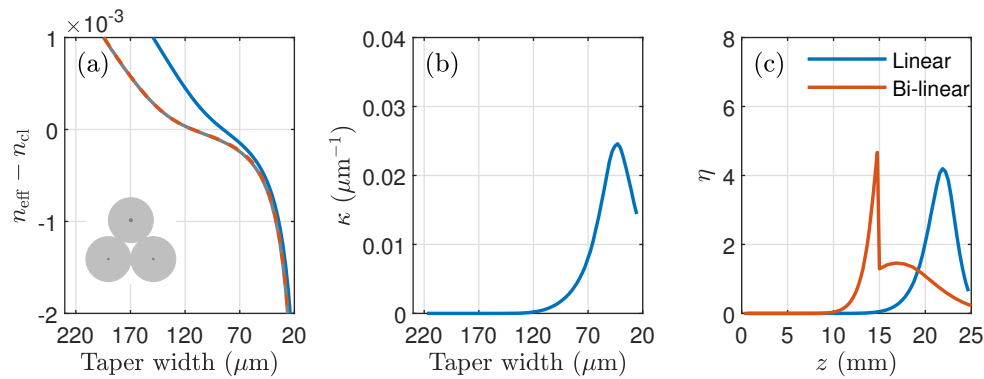


Fig. 16. (a) Effective index curves, (b) local coupling coefficient κ , and (c) the parameter η for an air-hole lantern taper with a cross-sectional structure shown in inset of (a). In comparison to the conventional lantern taper, the bi-linearity of the taper profile helps in decreasing the value of η .

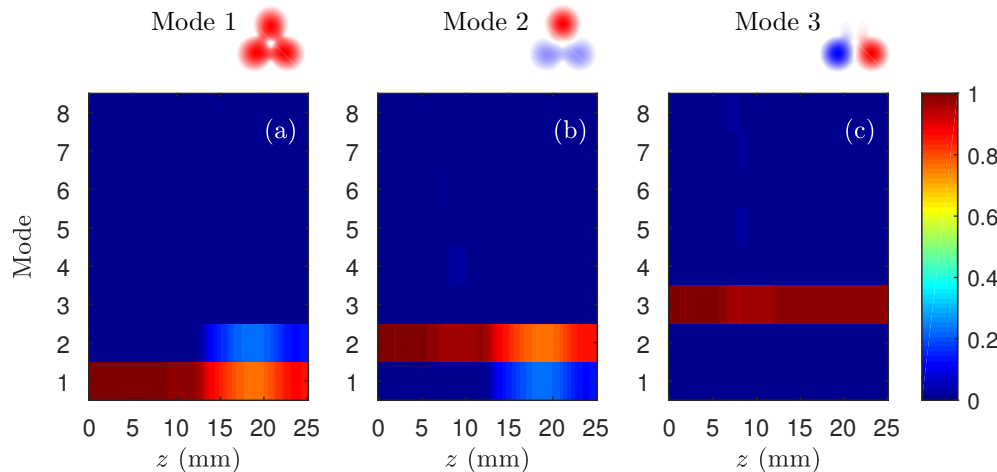


Fig. 17. Relative power distribution versus taper length in a 25-mm air-cladded lantern taper with an air hole between the three fibers. The initial light distribution is given by (a) eigenmode 1, (b) eigenmode 2, and (c) eigenmode 3.

Figure 17 shows the distributed modal power coupling for the 25-mm air-hole lantern taper. In comparison to Fig. 13 we observe a significant decrease in the crosstalk between mode 1 and mode 2, in agreement with the discussion above. The resulting crosstalk is -8.5 dB for light input in the SSMF (mode 1) and -11.5 dB for light input in either of the two HI1060 cores (average crosstalk of mode 2 and mode 3 input).

4.3. Discussion

While the simulations of the conventional lantern taper yielded high crosstalk values on the order of -3 dB, the introduction of a non-collapsed air hole between the three fibers strongly suppressed mode coupling and enabled crosstalk values below -8.5 dB. To the best of our knowledge, this is the first demonstration of such an air-gap effect in lantern tapers, which could potentially be used alongside graded- or logarithmic refractive index profiles to further mitigate

mode coupling in the taper [8,23,24]. Our finding also suggests that topology-optimized lanterns may present an interesting route for decreasing the length requirements for adiabatic conversion, especially in integrated photonic lanterns [25].

Even though the air gap was demonstrated to play an important role, the crosstalk values experimentally observed are still 3–6 dB smaller than numerically predicted. While this discrepancy may to some extent be attributed to uncertainties in fiber parameters, non-perfect taper transitions, or small diffusion of core dopants during tapering, another possible explanation may be that the dissimilar splice into the TMF, which was not included in the simulations, influences the crosstalk values. To investigate this, we included the TMF in our simulations at different alignment positions with respect to the taper. We found that both the modal crosstalk values and the mode-dependent loss depends strongly on the alignment position, in agreement with our experimental analysis. For one alignment position (3 μm vertical offset from center) the crosstalk values decrease to below -16 dB for all three input modes, albeit at the expense of higher losses (~ 2 & 6 dB) for the LP_{11} -like modes. This decrease in crosstalk is attributed to depend on the modal superposition at the end of the taper, the alignment offset in the dissimilar splice, and the final taper ratio. While further investigation of the effect of the splice offset is outside the scope of this paper, it is an important subject moving forward.

Finally, Fig. 17 indicates a small degree of internal crosstalk during the taper transition. As our measurement techniques only compare the input and output modes, it is not expected to capture such internal mode-interference effects, which would be detrimental for applications in optical communications and MDM. To investigate potential internal crosstalk, future work could include measurement of the full lantern transfer functions [5].

5. Conclusion

We have demonstrated a new fabrication technique for air-cladded photonic lanterns exhibiting low modal crosstalk of < -10 dB. The presented fabrication method is a cheaper alternative to the existing fabrication technique which uses a low index capillary tube. Using two types of single mode fibers, we could specifically excite the first two LP mode groups. Full-vectorial simulations of the structure, based on the eigenmode expansion method, revealed that a microscopic air gap, which was found between the three fibers, played an essential role in suppressing modal crosstalk. Combined with a gradual 25-mm long transition, a high degree of adiabatic mode conversion in the photonic-lantern taper was ensured. Further loss characterization also showed that the mode-dependent loss and measured crosstalk depends strongly on the alignment of the dissimilar splice to the two-mode fiber, and this was confirmed through numerical simulations. Finally, we note that the lack of a solid cladding makes the fabricated lanterns mechanically fragile. One way to improve this, while keeping fabrication costs low, is to coat a low refractive index UV curable polymer around the tapered end [10]. The fabrication of such polymer-cladded photonic lanterns, with a focus on optimizing the coating method to bring down optical losses, could be an interesting route moving forward.

Funding

The Danish Council for Independent Research Grant (DFF-4184-00433); Innovation Fund Denmark project (8057-00059B INCOM).

References

1. A. D. Ellis, J. Zhao, and D. Cotter, "Approaching the non-linear shannon limit," *J. Light. Technol.* **28**, 423–433 (2010).
2. D. J. Richardson, J. M. Fini, and L. E. Nelson, "Space-division multiplexing in optical fibres," *Nat. Photonics* **7**, 354–362 (2013).

3. R. Ryf, S. Randel, A. H. Gnauck, C. Bolle, A. Sierra, S. Mumtaz, M. Esmacelpour, E. C. Burrows, R.-J. Essiambre, P. J. Winzer, D. W. Peckham, A. H. McCurdy, and R. Lingle, "Mode-division multiplexing over 96 km of few-mode fiber using coherent 6 x 6 mimo processing," *J. Light. Technol.* **30**, 521–531 (2012).
4. C. Koebele, M. Salsi, D. Sperti, P. Tran, P. Brindel, H. Mardoyan, S. Bigo, A. Boutin, F. Verluise, P. Sillard, M. Astruc, L. Provost, F. Cerou, and G. Charlet, "Two mode transmission at 2x100gb/s, over 40km-long prototype few-mode fiber, using lcos-based programmable mode multiplexer and demultiplexer," *Opt. Express* **19**, 16593–16600 (2011).
5. S. G. Leon-Saval, N. K. Fontaine, J. R. Salazar-Gil, B. Ercan, R. Ryf, and J. Bland-Hawthorn, "Mode-selective photonic lanterns for space-division multiplexing," *Opt. Express* **22**, 1036–1044 (2014).
6. J. Love, W. Henry, W. Stewart, R. Black, S. Lacroix, and F. Gonthier, "Tapered single-mode fibers and devices .1. adiabaticity criteria," *IEE Proceedings-j Optoelectronics* **138**, 343–354 (1991).
7. D. Noordegraaf, P. M. Skovgaard, M. D. Nielsen, and J. Bland-Hawthorn, "Efficient multi-mode to single-mode coupling in a photonic lantern," *Opt. Express* **17**, 1988–1994 (2009).
8. B. Huang, N. K. Fontaine, R. Ryf, B. Guan, S. G. Leon-Saval, R. Shubochkin, Y. Sun, R. Lingle, and G. Li, "All-fiber mode-group-selective photonic lantern using graded-index multimode fibers," *Opt. Express* **23**, 224–234 (2015).
9. H. Liu, H. Wen, J. C. A. Zacarias, J. E. Antonio-Lopez, N. Wang, P. Sillard, R. Amezcua-Correa, and G. Li, "Demonstration of stable 3x10 gb/s mode group-multiplexed transmission over a 20 km few-mode fiber," in *Optical Fiber Communication Conference*, (Optical Society of America, 2018), p. W4J.2.
10. N. M. Mathew, L. Grüner-Nielsen, M. A. U. Castaneda, and K. Rottwitt, "A novel fabrication method for photonic lanterns," in *Optical Fiber Communication Conference*, (Optical Society of America, 2018), p. M4D.4.
11. N. M. Mathew, L. Grüner-Nielsen, M. A. U. Castaneda, M. Galili, and K. Rottwitt, "Mode-group selective air-clad photonic lantern," in *Frontiers in Optics / Laser Science*, (Optical Society of America, 2018), p. FTu5B.4.
12. S. G. Leon-Saval, N. K. Fontaine, and R. Amezcua-Correa, "Photonic lantern as mode multiplexer for multimode optical communications," *Opt. Fiber Technol.* **35**, 46–55 (2017).
13. D. J. DiGiovanni and D. M. Tipton, "Method for producing fused fiber bundles," (1999). US Patent 5,935,288.
14. Y. Zhu, E. Simova, P. Berini, and C. P. Grover, "A comparison of wavelength dependent polarization dependent loss measurements in fiber gratings," *IEEE Transactions on Instrumentation Meas.* **49**, 1231–1239 (2000).
15. L. Grüner-Nielsen, N. M. Mathew, and K. Rottwitt, "Direct measurement of polarization dependency of mode conversion in a long period grating," in *Optical Fiber Communication Conference (OFC) 2019*, (Optical Society of America, 2019), p. Th2A.15.
16. L. Gruner-Nielsen, N. M. Mathew, and K. Rottwitt, "Characterization of few mode fibers and devices," *Opt. Fiber. Technol.* (2019) to be published.
17. J. W. Nicholson, A. D. Yablon, J. M. Fini, and M. D. Mermelstein, "Measuring the modal content of large-mode-area fibers," *IEEE J. Sel. Top. Quantum Electron.* **15**, 61–70 (2009).
18. N. M. Mathew, L. Grüner-Nielsen, M. Galili, M. Lillieholm, M. A. U. Castaneda, and K. Rottwitt, "Polarization dependence of mode-group selective air-clad photonic lantern," in *Optical Fiber Communication Conference (OFC) 2019*, (Optical Society of America, 2019), p. Th3D.6.
19. Lumerical Solutions, Inc., <http://www.lumerical.com/tcad-products/mode/>.
20. G. V. Eleftheriades, A. S. Omar, L. P. B. Katehi, and G. M. Rebeiz, "Some important properties of waveguide junction generalized scattering matrices in the context of the mode matching technique," *IEEE Transactions on Microw. Theory Tech.* **42**, 1896–1903 (1994).
21. T. A. Birks, B. J. Mangan, A. Díez, J. L. Cruz, and D. F. Murphy, "Photonic lantern" spectral filters in multi-core fibre," *Opt. Express* **20**, 13996–14008 (2012).
22. S. Yerolatsitis, I. Gris-Sánchez, and T. Birks, "Adiabatically-tapered fiber mode multiplexers," *Opt. Express* **22**, 608–617 (2014).
23. K. Harrington, S. Yerolatsitis, D. V. Ras, D. M. Haynes, and T. A. Birks, "Endlessly adiabatic fiber with a logarithmic refractive index distribution," *Optica* **4**, 1526–1533 (2017).
24. J. C. Alvarado-Zacarias, N. K. Fontaine, J. E. Antonio-Lopez, Z. S. Eznavah, M. S. Habib, H. Chen, R. Ryf, D. Van Ras, P. Sillard, C. Gonnet *et al.*, "Mode selective photonic lantern with graded index core," in *Optical Fiber Communication Conference*, (Optical Society of America, 2018), p. M4D.5.
25. R. R. Thomson, T. A. Birks, S. Leon-Saval, A. K. Kar, and J. Bland-Hawthorn, "Ultrafast laser inscription of an integrated photonic lantern," *Opt. Express* **19**, 5698–5705 (2011).